

Polarization-analyzed resonant inelastic x-ray scattering of the orbital excitations in KCuF_3

K. Ishii,¹ S. Ishihara,^{2,3} Y. Murakami,^{1,2,4} K. Ikeuchi,^{1,4} K. Kuzushita,¹ T. Inami,¹ K. Ohwada,¹ M. Yoshida,¹ I. Jarrige,¹ N. Tatami,² S. Niioka,² D. Bizen,² Y. Ando,² J. Mizuki,¹ S. Maekawa,^{5,3} and Y. Endoh^{1,6}

¹*SPring-8, Japan Atomic Energy Agency, Hyogo 679-5148, Japan*

²*Department of Physics, Tohoku University, Sendai 980-8578, Japan*

³*CREST, Japan Science and Technology Agency (JST), Tokyo 102-0075, Japan.*

⁴*Institute of Materials Structure Science, Tsukuba 305-0801, Japan*

⁵*Advanced Science Research Center, Japan Atomic Energy Agency, Tokai 319-1195, Japan.*

⁶*International Institute for Advanced Studies, Kizu, Kyoto 619-0025, Japan*

(Dated: March 6, 2018)

We report a Cu K -edge resonant inelastic x-ray scattering (RIXS) study of orbital excitations in KCuF_3 . By performing the polarization analysis of the scattered photons, we disclose that the excitation between the e_g orbitals and the excitations from t_{2g} to e_g exhibit distinct polarization dependence. The polarization dependence of the respective excitations is interpreted based on a phenomenological consideration of the symmetry of the RIXS process that yields a necessary condition for observing the excitations. In addition, we show that the orbital excitations are dispersionless within our experimental resolution.

PACS numbers: 78.70.Ck, 75.25.Dk

Strongly correlated transition metal compounds attract great interest because of a variety of interesting properties such as high-temperature superconductivity in cuprates and colossal magnetoresistance in manganites [1]. It is widely recognized that the three degrees of freedom of the d electron, i.e., charge, spin, and orbital, play a crucial role in the occurrence of these phenomena. Hence spectroscopic investigations to measure the excitations of these degrees of freedom are required to elucidate their underlying interactions. Since intra-atomic d - d excitations are forbidden within the dipole approximation, spectroscopic methods other than the conventional optical measurement are highly demanded. In this respect, inelastic x-ray scattering (IXS) has proven to be an ideal candidate. In addition to the capability of observing dipole-forbidden transitions, IXS has a great advantage of also offering momentum resolution. Especially, one can explore a wide momentum range using IXS in the hard x-ray regime. A recent non-resonant IXS study showed that the d - d excitations can be observed at high momentum transfer [2], although non-resonant IXS usually suffers from low intensity. This shortcoming can be overcome by using resonant inelastic x-ray scattering (RIXS), where the incident photon energy is tuned near an absorption edge of a constituent element, resulting in a significant resonant enhancement of the electronic excitations [3, 4]. RIXS spectra are primarily related to the dynamical charge correlation [5, 6]. Furthermore, spin [7–9] and orbital [10, 11] excitations have also become accessible with the more recently developed spectrometers and their improved energy resolution.

In general, the RIXS spectrum is a function of energy, momentum, and polarization of both the incident and scattered photons. However, most RIXS studies so far have focused on energy and momentum dependences while the polarization, which is an inherent and

important character of the photon, was overlooked. Even though the role of the incident photon polarization was discussed in relation with the resonant conditions in a few experimental and theoretical works [12–16], the scattered photon polarization has not been identified at all. Like conventional Raman spectroscopy, polarization in RIXS must be connected to the symmetry of the excitations. Because the symmetry argument is rigorous and independent of the parameters in theoretical models, the polarization can be very useful for the assignment of the excitations in RIXS.

In this Letter, we conduct polarization analysis of the Cu K -edge RIXS of the orbitally-ordered compound KCuF_3 and demonstrate that the observation of the orbital (d - d) excitations by RIXS depends on the polarization conditions. KCuF_3 has long been known to display quantum one-dimensional antiferromagnetic properties along the c -axis originating from the strong superexchange interaction between the e_g orbitals of Cu^{2+} [18]. While the two e_g orbitals are degenerate under the cubic symmetry, in the real tetragonal structure the degeneracy is lifted, accompanied with the occurrence of strong Jahn-Teller distortions. The e_g orbitals are ordered according to the pattern shown in Fig. 1(a), which corresponds to an alternation of the hole orbitals $3d_{y^2-z^2}$ and $3d_{z^2-x^2}$ on adjacent Cu sites. There are two types of orbital excitations in KCuF_3 : One excitation is a transition of an electron from the t_{2g} orbital to the e_g orbital and the other one is between the e_g orbitals. The latter excitation is unique to the orbital-ordered Mott insulators. Utilizing our new polarization-analyzed RIXS technique, we have successfully measured the polarization dependence of these two types of orbital excitations and found that they are distinct from each other. The differences are interpreted based on a phenomenological group-theoretical consideration of RIXS, which gives the necessary polar-

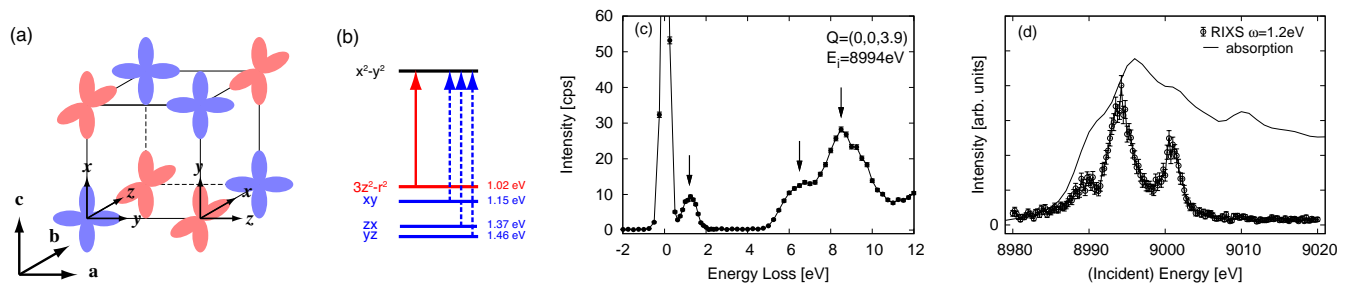


FIG. 1: (Color online) (a) Schematic representation of the orbital order of KCuF_3 in the hole picture. (b) Energy levels of the d electrons in KCuF_3 taken from E_{max} in Ref [17]. Solid and dashed arrows indicate the e_g excitation and t_{2g} excitations, respectively. (c) Typical RIXS spectrum of KCuF_3 . The vertical arrows indicate the peaks discussed in the text. (d) X-ray absorption spectrum of polycrystalline KCuF_3 (solid line) and RIXS intensity at 1.2-eV energy loss as a function of the incident energy.

ization conditions for observing each excitation. In the last part, we show that the orbital excitations are dispersionless within our experimental resolution.

The experiments were carried out at BL11XU at SPring-8. Incident x-rays were monochromatized by a double crystal Si(111) monochromator and a secondary Si(400) channel-cut monochromator. Scattered x-rays were analyzed in energy by a spherically bent Ge(733) crystal. When we performed polarization analysis of the scattered x-rays, a Ge(800) crystal was used instead of the Ge(733) one to keep space in the spectrometer for the polarization-analyzing device. The total energy resolution estimated from the full width at half maximum of the elastic peak was about 400 and 600 meV for the Ge(733) and Ge(800) crystals, respectively. For the polarization analysis of the scattered x-rays, a pyrolytic graphite (PG) crystal was placed in front of the detector and the (006) reflection of PG was measured. The scattering angle (θ_P) of the reflection at 8994 eV is 38° and the polarization extinction ratio ($\sin^2 2\theta_P$) is 0.94. Experimental reflectivity of the (006) reflection was about 0.02. By rotating the PG crystal and the detector about the axis of the beam, one can select the polarization of the scattered photon.

A single crystal of KCuF_3 was used. Polytype structures corresponding to different stacking of the ab -plane have been reported to exist in KCuF_3 [19]. Our single crystal was carefully prepared so that it only contains the (a)-type structure. This was confirmed by a magnetic susceptibility measurement where we observed a single antiferromagnetic transition at 38 K [20]. We use the Miller indices in the tetragonal unit cell of the primitive perovskite structure ($a = 4.1410 \text{ \AA}$ and $c = 3.9237 \text{ \AA}$) to represent the momentum transfer (\mathbf{Q}). The propagation vector of the orbital order is $(1/2, 1/2, 1/2)$. All the spectra were measured at room temperature.

A typical RIXS spectrum of KCuF_3 is shown in Fig. 1(c). The incident photon energy (E_i) is 8994 eV and the momentum transfer is $\mathbf{Q} = (0, 0, 3.9)$. Three peaks are observed at around 1.2, 6.5, and 8.5 eV, as indicated by the arrows in Fig. 1(c). The 1.2-eV peak corre-

sponds to orbital excitations which are the subject of this letter. A band structure calculation in the local density approximation including the on-site Coulomb interaction (LDA+U) suggested that KCuF_3 is a charge-transfer insulator rather than a Mott insulator [21]. Therefore we tentatively ascribe the 6.5-eV peak to a charge-transfer excitation from F $2p$ to Cu $3d$. It is noted that the calculated band gap is smaller than the energy loss of the RIXS peak. Using the analogy with copper oxides [22], we are tempted to ascribe the 8.5-eV peak to a molecular orbital excitation between bonding and antibonding states in a CuF_6 octahedron.

In Fig. 1(d), we show the resonant profile of the 1.2-eV excitation obtained by plotting the RIXS intensity at a fixed energy transfer (ω) of 1.2 eV as a function of E_i . The x-ray absorption spectrum (XAS) measured on a polycrystalline sample is superimposed. The resonant enhancement is found to occur for incident energies in the vicinity of the salient features of the XAS spectrum. Hereafter the incident photon energy is fixed at 8994 eV, where the intensity of the 1.2 eV excitation is maximum.

The polarization-analyzed RIXS spectra of the 1.2-eV feature are presented in Figs. 2 for four different crystal orientations schematized in the corresponding insets. The incident photon polarization (ϵ_i) lies in the scattering plane and the scattering angle (2θ) is chosen to be close to 90° in order to reduce the elastic scattering. The incident and scattered polarizations are therefore orthogonal to each other, which is the so-called the depolarized configuration. In each plot, the spectra are normalized so that the sum of the intensity of the $\pi \rightarrow \sigma'$ and $\pi \rightarrow \pi'$ inelastic signals is equal to the $\pi \rightarrow \sigma' + \pi'$ one. Here π is the incident photon polarization parallel to the scattering plane while π' and σ' denote the scattered photon polarizations parallel and perpendicular to the scattering plane, respectively. The most striking observation of this measurement is that additional intensity is found around 1 eV in the spectrum of $\pi \rightarrow \pi'$ compared with $\pi \rightarrow \sigma'$ in the configurations of (a) and (b), whereas the spectra in (c) and (d) are almost identical between the two polarization conditions. In a recent optical absorption study

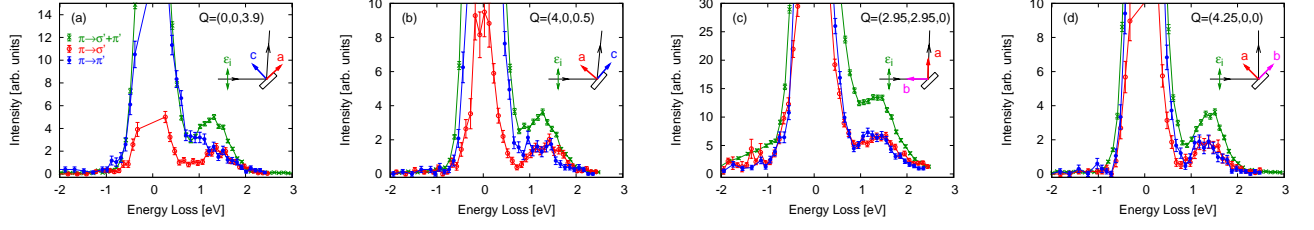


FIG. 2: (Color online) Polarization-analyzed RIXS spectra. Spectra with filled and open circles are measured in the $\pi \rightarrow \sigma'$ and $\pi \rightarrow \pi'$ conditions, respectively. The spectra without polarization analysis are also shown (crosses). Corresponding Experimental geometries are shown as inset.

[17, 23], the different orbital excitations were identified and their respective energies were estimated. The corresponding results are summarized in Fig. 1(b). Based on this assignment, we can ascribe the additional intensity at 1 eV to the excitation between the e_g orbitals (e_g excitation). Excitations from one of the t_{2g} orbitals to the unoccupied e_g orbital (t_{2g} excitations) are respectively located at 1.15, 1.37, and 1.46 eV in the optical absorption spectrum. These excitations are found to appear as a single peak in the RIXS spectrum within our resolution. While the t_{2g} excitations are observed for both polarization conditions in all four geometrical configurations, the e_g excitation appears only for the $\pi \rightarrow \pi'$ polarization of the configurations of Figs. 2 (a) and (b). This is a direct evidence that the e_g excitation has a different polarization dependence from the t_{2g} excitations.

The polarization conditions corresponding to the different geometrical configurations in Figs. 2 are summarized in Table I. The unit lattice vectors of the crystal are noted as \mathbf{a} , \mathbf{b} , and \mathbf{c} . The unit vectors \mathbf{x} , \mathbf{y} , and \mathbf{z} are taken so that the hole orbital is represented as $x^2 - y^2$. It is noted that there are two polarization conditions in the xyz coordinates because of the two orbital sublattices as illustrated in Fig. 1(a).

TABLE I: Summary of the polarization conditions of Fig. 2.

config.	polarization	ϵ_i	ϵ_f	symmetry of $P_i \times P_f$
(a)	$\pi \rightarrow \sigma'$	$\mathbf{y} + \mathbf{z}$	\mathbf{x}	$A_{2g} + B_{2g} + E_g$
	$(\mathbf{a} + \mathbf{c}) \rightarrow \mathbf{b}$	$\mathbf{x} + \mathbf{y}$	\mathbf{z}	E_g
	$\pi \rightarrow \pi'$	$\mathbf{y} + \mathbf{z}$	$\mathbf{y} - \mathbf{z}$	$A_{1g} + B_{1g} + E_g$
(b)	$(\mathbf{a} + \mathbf{c}) \rightarrow (\mathbf{a} - \mathbf{c})$	$\mathbf{x} + \mathbf{y}$	$\mathbf{x} - \mathbf{y}$	$B_{1g} + A_{2g}$
	$\pi \rightarrow \sigma'$	$\mathbf{y} + \mathbf{z}$	\mathbf{x}	$A_{2g} + B_{2g} + E_g$
	$(\mathbf{a} + \mathbf{c}) \rightarrow \mathbf{b}$	$\mathbf{x} + \mathbf{y}$	\mathbf{z}	E_g
(c)	$\pi \rightarrow \pi'$	$\mathbf{y} + \mathbf{z}$	$\mathbf{y} - \mathbf{z}$	$A_{1g} + B_{1g} + E_g$
	$(\mathbf{a} + \mathbf{c}) \rightarrow (\mathbf{a} - \mathbf{c})$	$\mathbf{x} + \mathbf{y}$	$\mathbf{x} - \mathbf{y}$	$B_{1g} + A_{2g}$
	$\pi \rightarrow \sigma'$	\mathbf{z}	\mathbf{y}	E_g
(d)	$\mathbf{a} \rightarrow \mathbf{c}$	\mathbf{y}	\mathbf{x}	$A_{2g} + B_{2g}$
	$\pi \rightarrow \pi'$	\mathbf{z}	\mathbf{x}	E_g
	$\mathbf{a} \rightarrow \mathbf{b}$	\mathbf{y}	\mathbf{z}	E_g
(d)	$\pi \rightarrow \sigma'$	$\mathbf{x} + \mathbf{z}$	\mathbf{y}	$A_{2g} + B_{2g} + E_g$
	$(\mathbf{a} + \mathbf{b}) \rightarrow \mathbf{c}$	$\mathbf{y} + \mathbf{z}$	\mathbf{x}	$A_{2g} + B_{2g} + E_g$
	$\pi \rightarrow \pi'$	$\mathbf{x} + \mathbf{z}$	$\mathbf{x} - \mathbf{z}$	$A_{1g} + B_{1g} + E_g$
	$(\mathbf{a} + \mathbf{b}) \rightarrow (\mathbf{a} - \mathbf{b})$	$\mathbf{y} + \mathbf{z}$	$\mathbf{y} - \mathbf{z}$	$A_{1g} + B_{1g} + E_g$

In order to interpret the difference between the polarization dependence of the e_g excitation and the t_{2g} excitations, we treat theoretically the polarization dependence of RIXS from a phenomenological view point, without identifying the microscopic scattering processes. The scattering cross section in RIXS is represented by the correlation function of the polarizability operator, corresponding to the S -matrix, as a function of momentum and the photon polarizations [24, 25]. This operator is expanded in terms of the excitation modes based on the group theoretical analyses. When the electronic excitations occur at the local site where the x-ray is absorbed, there is a selection rule for RIXS that a product-representation $\Gamma_i \times \Gamma_f \times P_i \times P_f$ should belong to the A_{1g} symmetry. Here $\Gamma_{i(f)}$ and $P_{i(f)}$ are the irreducible representations for the initial (final) electronic orbital and those of the incident (scattered) photon polarization, respectively. Equivalently, the excitations are allowed only if the product-representations $\Gamma_i \times \Gamma_f$ and $P_i \times P_f$ share at least one common symmetry. When other sites are involved in the electronic excitations, this selection rule is modified and depends on the momentum transfer \mathbf{Q} .

We approximately treat the local symmetry of the Cu atom as D_{4h} instead of the exact site symmetry of D_{2h} because the Cu-F distances along the x and y directions are almost equal. If only considering on-site excitations, the possible excitation modes in each polarization configuration of the measurements are given by $P_i \times P_f$. Those are listed in Table I. We also show the symmetry of the orbital excitations $\Gamma_i \times \Gamma_f$ in Table II. The symmetry of $P_i \times P_f$ has to be either A_{2g} or E_g for the observation of the t_{2g} excitation and either symmetry is always present in all four experimental configurations of Figs. 2. It means that the theoretical prediction agrees with the experimental results for the t_{2g} excitation. On the other hand, e_g excitation requires B_{1g} polarization symmetry,

TABLE II: Symmetry of the orbital excitations of KCuF_3 .

excitation	symmetry of $\Gamma_i \times \Gamma_f$
$(3z^2 - r^2) \rightarrow (x^2 - y^2)$	B_{1g}
$(xy) \rightarrow (x^2 - y^2)$	A_{2g}
$(yz) \rightarrow (x^2 - y^2)$	E_g
$(zx) \rightarrow (x^2 - y^2)$	E_g

which exists in the $\pi \rightarrow \pi'$ condition for the configurations of Figs. 2 (a), (b), and (d). Experimentally, the e_g excitation is observed in the $\pi \rightarrow \pi'$ condition for the configurations of Figs. 2 (a) and (b). The symmetry argument is again valid for the e_g excitation as long as it gives a necessary condition for its observation by RIXS. We briefly comment on the absence of the e_g excitation in the spectrum obtained in the $\pi \rightarrow \pi'$ condition of the configuration for Fig. 2 (d). From our symmetry analysis, the weight of the B_{1g} component for the $\pi \rightarrow \pi'$ polarization in the configuration of Fig. 2 (d) is deduced to be 40% of that for the $\pi \rightarrow \pi'$ polarization of Figs. 2 (a) and (b). For a quantitative agreement with the experiment, one may need to carry out a theoretical evaluation of the intensity including a microscopic description of the RIXS process.

We now turn to the momentum dependence of the orbital excitations. Because the orbital is an important degree of freedom through which novel properties of transition metal compounds can be controlled, the understanding of the elementary orbital excitation, so-called orbiton, is still a fascinating issue. Using Raman scattering, orbital excitation at zero momentum transfer has been observed in LaMnO_3 [26]. RIXS makes it feasible to probe the momentum dependence of this excitation [27]. Owing to our polarization analysis, we have been able to undoubtedly assign the 1 eV feature in the RIXS spectrum of KCuF_3 to the orbital degree of freedom of the system. We now present the momentum dependence of this excitation obtained for the whole Brillouin zone. Figures 3 (a) and (b) show the polarization-analyzed RIXS spectra obtained near the high-symmetry points of the Brillouin zone. Here \mathbf{q} is the momentum transfer in the reduced Brillouin zone. The spectra of the upper and lower three momenta in each figure are measured at or near the configurations of Fig. 2 (a) and (b), respectively.

In order to elucidate the dispersion relation of the orbital excitations quantitatively, we fitted the whole set of RIXS spectra in Figs. 3 (a) and (b). We start with the spectra collected with the $\pi \rightarrow \sigma'$ polarization in Fig. 3 (a), where only the t_{2g} excitation is observed. The tail of the elastic scattering or quasielastic component on the energy loss side was evaluated from the energy gain side. The excitation peak was approximated to a single Gauss function. We then fitted the spectra obtained in the $\pi \rightarrow \pi'$ condition in Fig. 3 (b), using the peak positions and widths of the t_{2g} excitation inferred from the fits of the spectra in Fig. 3 (a) and keeping them fixed. The peak centers and FWHMs used in the fits are plotted as functions of the reduced momentum transfer in Fig. 3 (c). The dispersion relation of the excitations is small. It is noteworthy that the dispersion of this excitation between the two e_g orbitals, which corresponds to the orbital order in KCuF_3 , is not discernible within the experimental resolution. This result suggests that the Jahn-Teller splitting between the two e_g orbitals is about 1 eV irrespective of the momentum transfer. Moreover, we conclude that the inter-site interactions between the

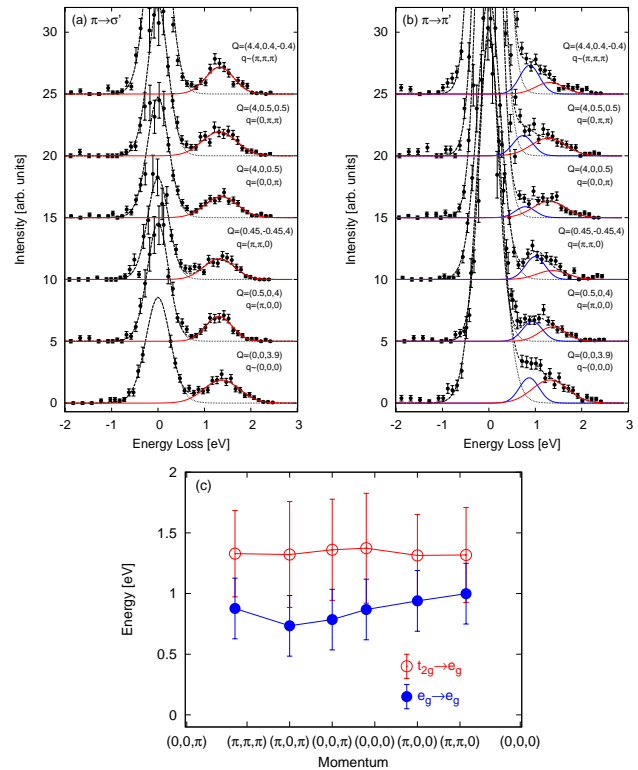


FIG. 3: (Color online) (a) and (b) Momentum dependence of polarization-analyzed RIXS spectra. \mathbf{Q} and \mathbf{q} are the absolute momentum transfer and the reduced one, respectively. The filled circles correspond to the experimental data and solid-line spectra are the fitted orbital excitations. Dashed-line spectra represent the sum of the fitted elastic line (dotted line) with the fitted orbital excitations (solid line). (c) Dispersion relation of the orbital excitations. The peak positions are indicated by the circles and the bars denote the FWHM of the excitations.

d orbitals, which can be ascribed to the magnitude of the dispersion, are much smaller in energy than the experimental resolution (600 meV). Overall, these data importantly show that RIXS at the K -edge can be used as a robust technique that provides information about the dependence of the electronic excitations upon two key parameters of the condensed matter physics, momentum and polarization. Since improvement of the energy resolution is still in progress, the dispersion relation of orbital excitations should become observable by K -edge RIXS in the near future.

In summary, we have performed a polarization-analyzed resonant inelastic x-ray scattering study of the orbital excitations in KCuF_3 at the Cu K -edge. The polarization of the scattered photons in RIXS was identified for the first time. A clear contrast is found in the polarization dependence between the excitation between the e_g orbitals and the excitations from the t_{2g} orbitals to the e_g orbital. The former excitation is observed in the $\pi \rightarrow \pi'$ polarization for two of the four studied geometrical configurations, while the latter appears in both

$\pi \rightarrow \pi'$ and $\pi \rightarrow \sigma'$ polarizations for all four configurations. The polarization dependence of both orbital excitations can be understood based on the symmetry of the RIXS process, which gives a necessary condition for the appearance of these orbital excitations. We measured the momentum dependence of the polarization-analyzed excitations and found that both orbital excitations are

nearly dispersionless within our experimental resolution.

This work was performed under the inter-university cooperative research program of the Institute of Materials Research, Tohoku University and financially supported by the Grant-in-Aid for Young Scientists (B) (No. 20740179) from JSPS.

-
- [1] S. Maekawa *et al.*, *Physics of Transition Metal Oxides* (Springer, 2004).
- [2] B. C. Larson *et al.*, Phys. Rev. Lett. **99**, 026401 (2007).
- [3] A. Kotani *et al.*, Rev. Mod. Phys. **73**, 203 (2001).
- [4] M. Z. Hasan *et al.*, Science **288**, 1811 (2000).
- [5] K. Ishii *et al.*, Phys. Rev. Lett. **94**, 207003 (2005).
- [6] J. Kim *et al.*, Phys. Rev. B **79**, 094525 (2009).
- [7] J. P. Hill *et al.*, Phys. Rev. Lett. **100**, 097001 (2008).
- [8] L. Braicovich *et al.*, Phys. Rev. Lett. **102**, 167401 (2009).
- [9] J. Schlappa *et al.*, Phys. Rev. Lett. **103**, 047401 (2009).
- [10] Y.-J. Kim *et al.*, Phys. Rev. B **69**, 155105 (2004).
- [11] C. Ulrich *et al.*, Phys. Rev. Lett. **103**, 107205 (2009).
- [12] K. Hämäläinen *et al.*, Phys. Rev. B **61**, 1836 (2000).
- [13] T. Idé *et al.*, J. Phys. Soc. Jpn. **69**, 3107 (2000).
- [14] L. Lu *et al.*, Phys. Rev. B **74**, 224509 (2006).
- [15] M. Takahashi, *et al.*, J. Phys. Soc. Jpn. **77**, 034711 (2008).
- [16] F. Vernay *et al.*, Phys. Rev. B **77**, 104519 (2008).
- [17] J. Deisenhofer *et al.*, Phys. Rev. Lett. **101**, 157406 (2008).
- [18] K. Hirakawa *et al.*, J. Phys. Soc. Jpn. **23**, 756 (1967).
- [19] A. Okazaki, J. Phys. Soc. Jpn. **26**, 870 (1969).
- [20] M. T. Hutchings *et al.*, Phys. Rev. **188**, 919 (1969).
- [21] N. Binggeli *et al.*, Phys. Rev. B **70**, 085117 (2004).
- [22] Y.-J. Kim *et al.*, Phys. Rev. B **70**, 205128 (2004).
- [23] In general, electric dipole transitions between d orbitals are parity-forbidden but they can become allowed by assistance of phonons.
- [24] S. Ishihara *et al.*, Phys. Rev. B **62**, R9252 (2000).
- [25] S. Ishihara, *et al.*, Physica B **345**, 15 (2004).
- [26] E. Saitoh *et al.*, Nature **410**, 180 (2001).
- [27] S. Ishihara *et al.*, Phys. Rev. B **62**, 2338 (2000).